J. Marine Sci. Appl. (2017) 16:
DOI: https://doi.org/10.1007/s11804-017-1436-4

Monolithic Coupling of the Pressure and Rigid Body Motion Equations in Computational Marine Hydrodynamics

Hrvoje Jasak, Inno Gatin* and Vuko Vukčević

Faculty of Mechanical Engineering and Naval Architecture, University of Zagreb, 10000 Zagreb, Croatia

Abstract: In Fluid Structure Interaction (FSI) problems encountered in marine hydrodynamics, the pressure field and the velocity of the rigid body are tightly coupled. This coupling is traditionally resolved in a partitioned manner by solving the rigid body motion equations once per nonlinear correction loop, updating the position of the body and solving the fluid flow equations in the new configuration. The partitioned approach requires a large number of nonlinear iteration loops per time–step. In order to enhance the coupling, a monolithic approach is proposed in Finite Volume (FV) framework, where the pressure equation and the rigid body motion equations are solved in a single linear system. The coupling is resolved by solving the rigid body motion equations once per linear solver iteration of the pressure equation, where updated pressure field is used to calculate new forces acting on the body, and by introducing the updated rigid body boundary velocity in to the pressure equation. In this paper the monolithic coupling is validated on a simple 2D heave decay case. Additionally, the method is compared to the traditional partitioned approach (*i.e.* "strongly coupled" approach) in terms of computational efficiency and accuracy. The comparison is performed on a seakeeping case in regular head waves, and it shows that the monolithic approach achieves similar accuracy with fewer nonlinear correctors per time–step. Hence, significant savings in computational time can be achieved while retaining the same level of accuracy.

Keywords: monolithic coupling, pressure equation, rigid body motion, computational fluid dynamics, marine hydrodynamics, seakeeping

1 Introduction

In computational marine hydrodynamics, the problems including Fluid Structure Interaction (FSI) involving floating bodies are often encountered. Furthermore, elasticity of the body can be neglected in most applications, modelling only six degrees of freedom for the rigid body motion. In majority of cases, the problem includes a body at the free surface, forced into motion by wave forces or initial non–equilibrium of mass and displaced volume. In either case, the oscillatory motion of the floating body is primarily a result of interplay of pressure forces acting on the body, and the gravitational force. Since the fluid is incompressible, the pressure field is sensitive to the change in the body velocity. For this reason, this paper focuses on the coupling of the pressure equation and rigid body motion equations. The coupling is performed monolithically, where the pressure equation and rigid body motion equations are solved simultaneously. The development is performed in Naval Hydro software pack based on foam–extend open–source software.

Monolithic solution strategy is well documented in the literature for FSI involving deformable bodies, where the fluid and the structure are modelled within the same spatial discretisation framework (Hachem *et al.*, 2013; Legay *et al.*, 2011), or on separate grids (Farah *et al.*, 2016; Hu *et al.*, 2016). Finite Element Method is mostly used to discretise the structure and fluid flow equations (Bna *et al.*, 2013; Farah *et al.*, 2016; Hachem *et al.*, 2013; Heil *et al.*, 2008; Jog and Pal, 2011; Langer and Yang, 2016; Legay *et al.*, 2011; Yang *et al.*, 2016), while FV is used in some publications (Eken and Sahin, 2016; Hu *et al.*, 2016). Some authors state that the monolithic FSI model with a discretised structure can calculate rigid body dynamics as a special case. Hachem *et al.* (2013) state that the rigid body can be modelled by imposing special conditions to the Navier–Stokes equations for the stencils inside the structure. Legay *et al.* (2011) and Robinson-Mosher *et al.* (2011) show that rigid body can be simulated within the presented model by substituting the structural system of equations with the rigid body motion equations.

The publications mentioned above discretise the structure in order to provide a general framework for deforming bodies. In case of rigid bodies, the discretisation of the body volume would present an unnecessary overhead. Integrating the rigid body motion equations only requires information of mass, angular inertia of the body, and relative position of the centre of gravity, which are constant.

The novelty of this work is in the monolithic approach to the pressure–rigid body motion coupling within the FV framework where the body is represented as a boundary of the fluid domain, while the volume inside the body is not discretised. The approach offers a more resolved solution of the coupling comparing to the widely used partitioned approach (Orihara and Miyata, 2003; Castiglione *et al.*, 2011;

Received date: 10-Jan-2017
Accepted date: 28-Jul-2017
*Corresponding author Email: inno.gatin@fsb.hr

Wu *et al.*, 2011; Simonsen *et al.*, 2013; Vukčević and Jasak, 2015a; Simonsen *et al.*, 2013; Tezdogan *et al.*, 2015; Miyata *et al.*, 2014), enabling a reduction of the number of nonlinear iterations per time–step. In the present approach, the pressure field and the solid body motion equations are coupled at the level of linear solver step of the pressure equation. After each linear solver iteration, the updated pressure field is used to calculate forces acting on the rigid body, which are in turn used to repeatedly integrate the solid body motion equations. The updated velocity of the solid body is then injected in the right hand side of the pressure equation as the change of volumetric flux at the body boundary.

The paper is organized as follows. First, the numerical model is presented, comprising the discretisation of the coupling of the pressure equation and the rigid body motion equations, followed by details regarding the linear solver and the Aitkens relaxation method. Next, validation of the present approach is performed on a 2D heave decay test case by comparing with the well established partitioned approach. In the fourth section the two methods are compared on a seakeeping case in regular head waves. Finally, an overview of results and conclusion are given.

2 Numerical model

In this section the mathematical and numerical formulation of the monolithic coupling of the pressure equation and rigid body motion equation is described.

The momentum equation or incompressible, two phase flow states (Vukčević *et al.*, 2016a):

$$\frac{\partial \boldsymbol{u}}{\partial t} + \nabla . ((\boldsymbol{u} - \boldsymbol{u}_M)\,\boldsymbol{u}) - \nabla . (\nu_e \nabla \boldsymbol{u}) = -\frac{1}{\rho}\nabla p_d \tag{1}$$

where $\boldsymbol{u}$ stands for the velocity field, while $\boldsymbol{u}_M$ is the relative grid motion velocity accounting for the Space Conservation Law (Demirdžić and Perić, 1988). ν_e stands for the effective kinematic viscosity, ρ is the density, while p_d stands for the dynamic pressure: $p_d = p - \rho \boldsymbol{g} . \boldsymbol{x}$, where $\boldsymbol{g}$ denotes the gravitational constant, while $\boldsymbol{x}$ represents the radii vector.

The pressure equation is derived from the mass conservation law, which can be written in the following form for incompressible flow:

$$\nabla . \boldsymbol{u} = 0 \tag{2}$$

The change of the boundary velocity $\delta \boldsymbol{u}_b$ of the rigid body can be accounted for explicitly in the continuity equation as:

$$\nabla . \boldsymbol{u} + \nabla . (\delta \boldsymbol{u}_b) = 0 \tag{3}$$

The discretisation of Eq. (2) in the integral FV framework will be omitted for brevity, the reader is directed to Jasak (1996) for details. The discretisation of Eq. (2) yields the pressure equation, which can be written in the form:

$$\sum_f \boldsymbol{s}_f . \left(\frac{1}{a_P}\right)_f \left(\frac{\nabla p_d}{\rho}\right)_f = \sum_f \boldsymbol{s}_f . \frac{(\boldsymbol{H}(\boldsymbol{u}_N))_f}{(a_P)_f} \tag{4}$$

where f denotes the face index, $\boldsymbol{s}_f$ stands for the surface area vector: $\boldsymbol{s}_f = s_f \boldsymbol{n}$, where s_f stands for the area of the face, while $\boldsymbol{n}$ denotes the face unit normal vector. a_P is the diagonal coefficient from the discretised momentum equation, Eq. (1) (Jasak, 1996). $\boldsymbol{H}$ is a linear operator stemming from the discretisation of the momentum equation, which is a function of explicit neighbouring cell velocities $\boldsymbol{u}_N$. The discretisation of the divergence of change of the boundary velocity in integral form states:

$$\int_V \nabla . (\delta \boldsymbol{u}_b) \mathrm{d}V = \oint_S \boldsymbol{n} . \delta \boldsymbol{u}_b \mathrm{d}S = \sum_f \boldsymbol{s}_f . \delta \boldsymbol{u}_{bf} \tag{5}$$

where the Gauss's theorem is employed to transform the volume integral into a surface integral. The final discretised form of the pressure equation monolithically coupled with the rigid body motion states:

$$\begin{aligned} &\sum_f \boldsymbol{s}_f . \left(\frac{1}{a_P}\right)_f \left(\frac{\nabla p_d}{\rho}\right)_f = \\ &\sum_f \boldsymbol{s}_f . \frac{(\boldsymbol{H}(\boldsymbol{u}_N))_f}{(a_P)_f} - \sum_f \boldsymbol{s}_f . \delta \boldsymbol{u}_{bf} \end{aligned} \tag{6}$$

The last term on the right hand side of Eq. (6) provides the coupling between the pressure equation and the rigid body motion. Note that mathematically, u_{bf} presents a velocity field defined at face centres, with non–zero values only where only for faces at the rigid body boundary.

To obtain the change of velocity $\delta \boldsymbol{u}_b$, rigid body motion equations are integrated:

$$\begin{aligned} \frac{\partial \boldsymbol{v}}{\partial t} &= \boldsymbol{F}/m \\ \frac{\partial \boldsymbol{\omega}}{\partial t} &= \boldsymbol{I}^{-1} . (\boldsymbol{M} - \boldsymbol{\omega} \times (\boldsymbol{I} . \boldsymbol{\omega})) \end{aligned} \tag{7}$$

where $\boldsymbol{v}$ denotes the translational velocity of the centre of mass, $\boldsymbol{F}$ is the total exerted force on the body, while m stands for the mass of the body. $\boldsymbol{\omega}$ is the rotational velocity, $\boldsymbol{I}$ is the tensor of inertia, while $\boldsymbol{M}$ stands for the external moment acting on the body. The force and moment acting on the body are calculated as the sum of pressure and viscous forces:

$$\begin{aligned} \boldsymbol{F} &= \sum_{bf} \boldsymbol{s}_{bf} p_{bf} + \boldsymbol{F}_v \\ \boldsymbol{M} &= \sum_{bf} \boldsymbol{r}_{bf} \times \boldsymbol{s}_{bf} p_{bf} + \boldsymbol{M}_v \end{aligned} \tag{8}$$

where the summation is carried out on boundary faces denoted with index bf, while $\boldsymbol{F}_v$ and $\boldsymbol{M}_v$ denote the viscous portion of the force and moment, respectively. The pressure at the boundary face p_{bf} is calculated from the dynamic pressure as: $p_{bf} = p_{d,bf} + \rho \boldsymbol{g} . \boldsymbol{x}_{bf}$. Hence, it represents the cross coupling term with the pressure equation, Eq. (6). The change of the boundary velocity $\delta \boldsymbol{u}_{bf}$ is finally calculated as the change of the translational and rotational velocity of the boundary face bf in the two adjacent linear solver iterations:

$$\delta \boldsymbol{u}_{bf}^n = \boldsymbol{v}^n - \boldsymbol{v}^{n-1} + (\boldsymbol{\omega}^n - \boldsymbol{\omega}^{n-1}) \times \boldsymbol{x}_{bf} \tag{9}$$

where n denotes the linear solver iteration, while $\boldsymbol{x}_{bf}$ denotes the radii vector of the boundary face.

Eq. (6) to Eq. (9) present a closed system regarding the pressure–rigid body motion coupling. At linear solver iteration level the following algorithm is employed to conduct the coupling:

1) Initialize $\delta \boldsymbol{u}_{bf}$ to zero,
2) Perform one iteration of the linear solver for the dynamic pressure equation, Eq. (6),
3) Update the dynamic pressure p_d,
4) Calculate the new forces and moments, Eq. (8), while keeping the viscous portion of the force constant,
5) Integrate the rigid body motion equations, Eq. (7),
6) Calculate the change of the boundary velocity, Eq. (9).
7) Go to next linear solver iteration,
8) Repeat 2) to 7) until convergence.

A flow chart of the nonlinear corrector used in this work is shown on Fig. 1. Note that multiple pressure corrections are performed in one nonlinear corrector.

In the two phase flow solver, Ghost Fluid Method is used (Vukčević, 2016) to impose the free surface boundary conditions in the FV framework, while Spectral Wave Explicit Navier Stokes Equations (SWENSE) (Vukčević *et al.*, 2016a) is used to imposed the wave field in the CFD domain.

2.1 Linear solver and rigid body motion integration

In this work the discretised pressure equation is solved using a preconditioned Conjugate Gradient (Saad, 2003) method for sparse linear systems. Cholesky factorisation is used as a preconditioner.

Integration of rigid body motion equations is performed using Fifth-order Cash-Karp embedded Runge-Kutta scheme with error control and adjustive time-step size (Press *et al.*, 2002).

2.2 Aitkens relaxation

In order to stabilise the calculation of the rigid body motion, Aitken's adaptive relaxation (Irons and Tuck, 1969) is employed. Since the solution of the pressure can vary dramatically in the first several iterations of the linear solver, the coupling with the rigid body motion equations can be unstable. In order to circumvent the instability, a dynamic relaxation is needed to exert heavy relaxation at the beginning of the linear solution process, and gradually increase the relaxation factor as the pressure solution starts to converge.

Using Aitken's algorithm, the acceleration of translational and rotational motion is relaxed. Here, the algorithm will be presented only for translational acceleration $\boldsymbol{a}$ for brevity. Acceleration $\boldsymbol{a}_k$ of the kth iteration is obtained using the relaxation factor ω_k:

$$\boldsymbol{a}_k = (1 - \omega_k)\,\widetilde{\boldsymbol{a}}_k + \omega_k \boldsymbol{a}_{k-1} \tag{10}$$

where tilde denotes the calculated value. The relaxation factor is calculated based on the information from the previous

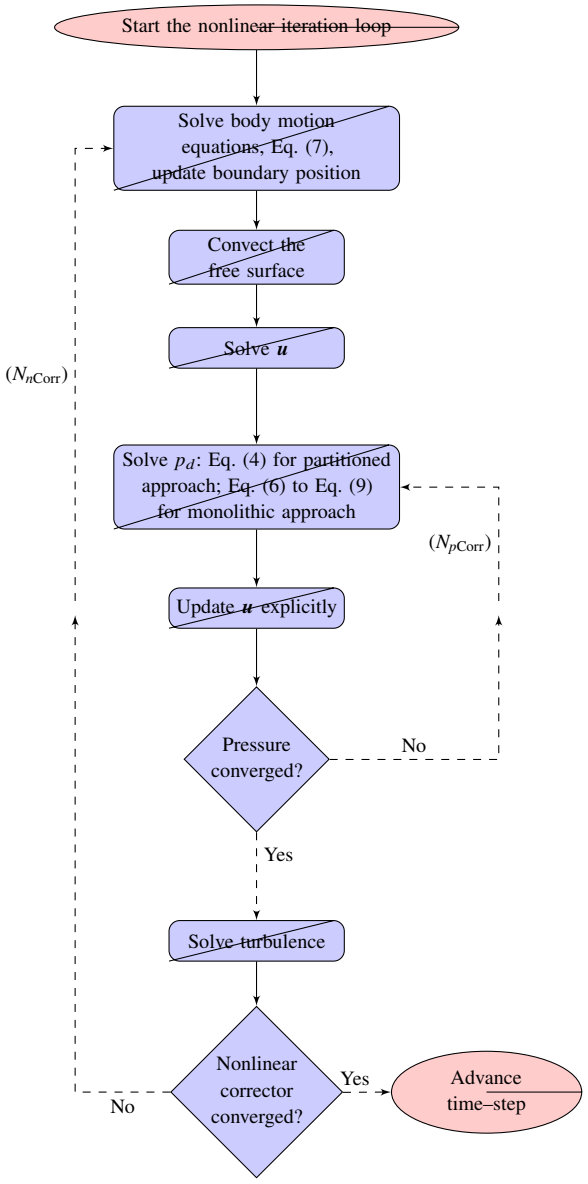

Fig. 1 Flow chart of the nonlinear corrector

iterations:

$$\omega_k = \omega_{k-1} + (\omega_{k-1} - 1)\,\frac{(\Delta \boldsymbol{a}_{k-1} - \Delta \boldsymbol{a}_k)\cdot \Delta \boldsymbol{a}_k}{(\Delta \boldsymbol{a}_{k-1} - \Delta \boldsymbol{a}_k)^2} \tag{11}$$

where $\Delta \boldsymbol{a}_k = \boldsymbol{a}_{k-1} - \boldsymbol{a}_k$, while $\Delta \boldsymbol{a}_{k-1} = \boldsymbol{a}_{k-2} - \boldsymbol{a}_{k-1}$.

3 Heaving barge test case

In this section the novel monolithic coupling of the pressure equation and rigid body motion is validated on 2D heave decay case of a barge. The results are compared with the partitioned approach, where the rigid body motion equations are updated once per nonlinear correction loop.

The 2D floating barge is set above the hydrostatic equilibrium position by 0.01 m at time zero to produce a heave decay motion. The mass of the barge is 0.32 kg, with height of 0.12 m, width of 0.2 m, and draught of 0.08 m. 32 160 cells are used for both the monolithic and

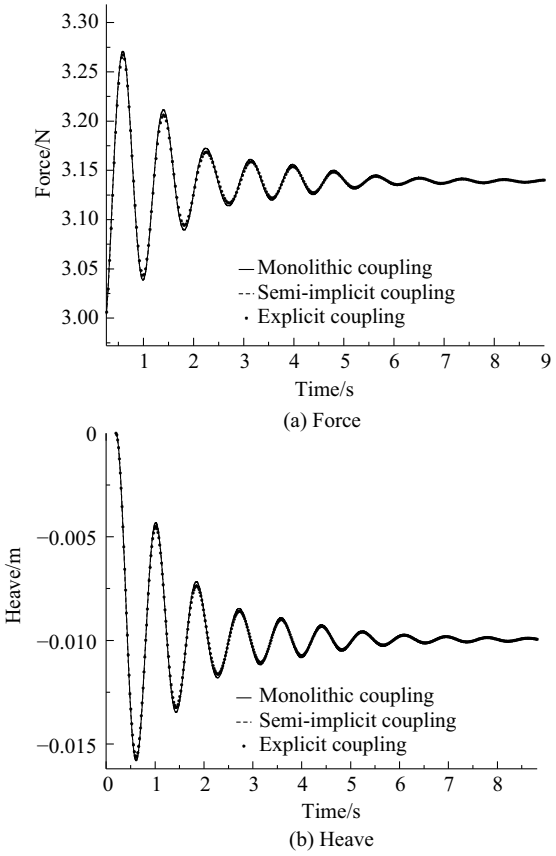

Fig. 2 Comparison of the force signal and heave motion for the 2D heave decay case

partitioned simulation, while a fixed time step of 0.001 42 s is set corresponding to ≈ 400 time–steps per natural period of oscillation. The number of time–steps per period of oscillation is selected based on the authors experience, which can be found in Vukčević *et al.* (2016). The same number of nonlinear correctors is used per time–step, as well as the number of pressure corrections per nonlinear loop in every simulation. Eight nonlinear correctors per time–step and four pressure correctors per each nonlinear loop are used. The domain is 2 meters wide, 0.5 meters deep beneath the free surface and 0.5 meters high above the free surface. The computational grid is rigidly moving together with the moving body. Fixed zero value boundary condition for velocity is prescribed on the side boundaries and bottom, while a mixed fixed value and zero gradient boundary condition is placed at the top boundary. For pressure, zero gradient is placed on sides and bottom, while fixed value is set on the top boundary. For the VOF field, zero gradient boundary condition is placed on all boundaries.

For discretisation of the temporal term in the momentum equation backward second order scheme is used, while implicit upwind scheme with deferred second order correction is used for the convection term. The diffusion term in momentum equation, and the pressure equation are discretised using second order accurate scheme with explicit non–orthogonal correction. Same discretisation is used in all

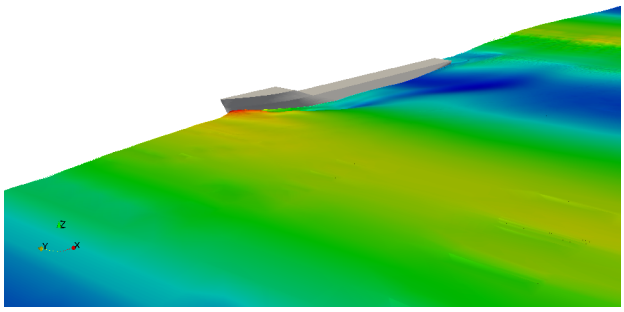

Fig. 3 Perspective view of the seakeeping simulation

calculations performed for this study.

The results are shown in Fig. 2, where the time signal of vertical force acting on the barge and heave motion are shown for the two simulations. Results of the monolithic coupling approach show good agreement with the partitioned approach, which validates the novel monolithic approach since the partitioned approach has been validated (Vukčević and Jasak, 2015a; Vukčević and Jasak, 2015b; Vukčević *et al.*, 2016b).

4 Seakeeping test case

A comparison of seakeeping simulation results is shown in this section for partitioned and novel monolithic approach. The convergence of the results with respect to the number of nonlinear correctors per time–step and the number of pressure correctors per each nonlinear corrector is compared, as well as computational demands.

Seakeeping simulation for the KRISO Container Ship (KCS) model in regular head waves is simulated (Fig. 3), where the simulation set–up corresponds to the C5 case from the Tokyo Workshop on CFD in Ship Hydrodynamics (Larsson *et al.*, 2015). Simulations are performed in model scale for Froude number $Fr = 0.261$, with length $L_{PP} = 6.05\,\text{m}$, breadth $B = 0.85\,\text{m}$ and drought $T = 0.285\,\text{m}$. Regular incident wave is imposed with wave length $\lambda = 11.84\,\text{m}$ and wave height $H = 0.196\,\text{m}$. Relatively coarse grid is used with 600 000 cells to discretise half of the domain. Implicit relaxation zones Jasak *et al.*, (2015) are used to initialize the waves at the inlet boundary, and to damp the waves at the outlet. The inlet boundary is at a distance of $1L_{PP}$ in front of the bow, while the outlet is $2L_{PP}$ from the aft perpendicular. Side boundary is placed at $1.5L_{PP}$ from the centre line of the ship, while the depth of the domain is set to $1.5L_{PP}$ and height above the free surface to $1L_{PP}$. The ship is free to heave and pitch, while the surge velocity is set to a constant value. Eight simulations are performed altogether, where the number of nonlinear correctors per time–step and number of pressure correctors per nonlinear corrector in individual simulation are shown in the test matrix, Table 1.

Table 1 The test matrix showing the number of nonlinear correctors, $N_{n\text{Corr}}$ per time–step and the number of pressure correctors, $N_{p\text{Corr}}$ per each nonlinear corrector for each simulation

Simulation No.	$N_{n\text{Corr}}$	$N_{p\text{Corr}}$
1	2	2
2	2	4
3	2	8
4	4	4
5	6	4
6	8	4
7	10	4
8	14	4

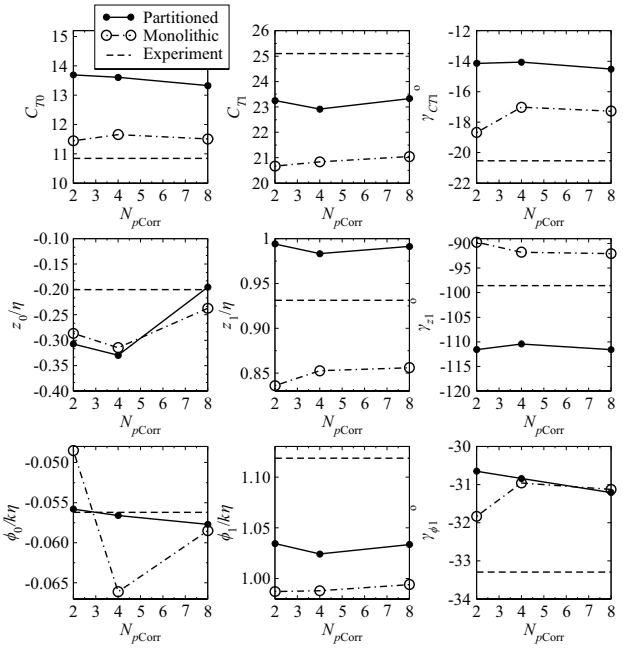

Fig. 4 Comparison of seakeeping results of partitioned and monolithic approach for coupling body motion and pressure equation, with respect to the number of pressure corrections $N_{p\text{Corr}}$

Fig. 4 shows the comparison of results of the two different coupling strategies with respect to the number of pressure corrections per nonlinear corrector, $N_{p\text{Corr}}$ (see Fig. 1). The results correspond to simulations 1, 2 and 3 from Table 1. Hereafter, C_T stands for total resistance coefficient, z is heave, ϕ is pitch. η stands for wave amplitude, while k stands for the wave number. Mean values of harmonic oscillations in time are indicated with index 0, and first order amplitudes with 1.

is the phase shift of the item indicated in the index. The first row of graphs shows, from left to right, the mean, first order amplitude and first order phase shift of the resistance coefficient. The second row shows the dimensionless heave motion, while the third shows the dimensionless pitch motion. Experimental data from Tokyo Workshop on CFD in Ship

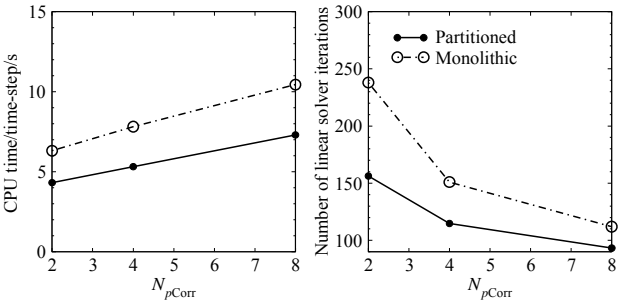

Fig. 5 Comparison of required computational time per time–step and the average number of pressure equation iterations with respect to the number of pressure corrections $N_{p\text{Corr}}$

Hydrodynamics (Larsson *et al.*, 2015) is also included for reference, however the reader is referred to Vukčević and Jasak (2015a) and Vukčević and Jasak (2015b) for detailed validation of seakeeping with finer grids. The partitioned approach differs significantly from the monolithic approach for most items. The cause is that two nonlinear correctors per time–step are not sufficient for the partitioned approach to produce accurate results. This is further demonstrated on Fig. 6, where the partitioned approach exhibits a large variation in results obtained using 2, 4, 6, 8, 10 and 14 nonlinear correctors per time–step. The partitioned approach does not update the rigid body motion equations inside the pressure loop, *i.e.* the number of rigid body motion updates per time–step does not depend on $N_{p\text{Corr}}$. Hence, the variation of results with changing number of $N_{p\text{Corr}}$ is due to the unresolved fluid flow solution. For most items the results obtained using the partitioned approach show very little dependence on $N_{p\text{Corr}}$, except for the mean value of heave, z_0. Hence, it can be concluded that the mean value of heave is sensitive to the accuracy of the pressure field solution. The monolithic approach shows dependence on $N_{p\text{Corr}}$ for more items ($_{CT1}$, ϕ_0, $_{\phi 1}$), since increasing the number of pressure corrections improves the coupling between the pressure force and rigid body motion. On Fig. 5 the average computational time per time–step is compared for the two approaches with respect to the number of pressure correctors per nonlinear corrector, as well as the average number of pressure equation linear solver iterations. As expected, the monolithic approach takes more computational time per time–step than partitioned approach, which is caused by solving the rigid body motion equations once per pressure linear solver iteration. Also, higher number of linear solver iterations is required, which can be prescribed to the fact that the source of the system of equations is changing throughout the solution process.

Fig. 6 shows the comparison of results for the two approaches with respect to the number of nonlinear correctors per time–step. The results correspond to simulations with indices 2 and 4 to 8 from Table 1. Again, experimental data is included for reference. Most items exhibit differences within 10%, while some exhibit higher differences. It should

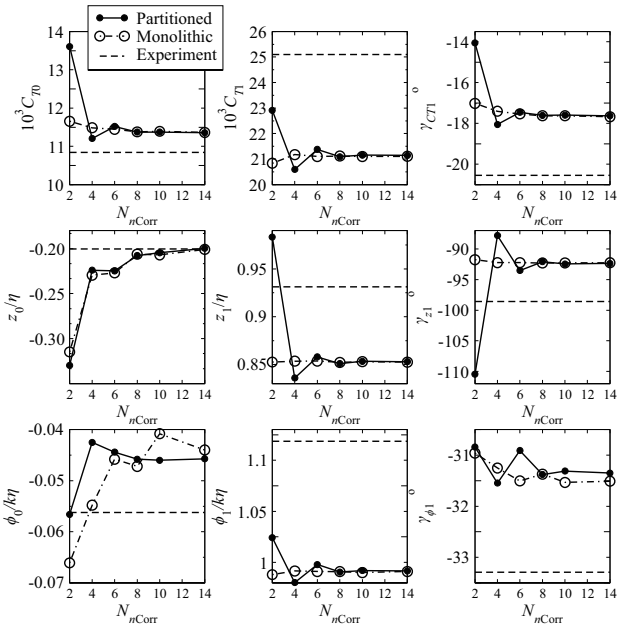

Fig. 6 Comparison of seakeeping results of partitioned and monolithic approach for coupling body motion and pressure equation, with respect to the number of nonlinear correctors per time–step $N_{n\mathrm{Corr}}$

be noted here that the focus of this paper is not on validation of seakeeping, rather on proving the benefits of the monolithic coupling. Hence, coarse spatial resolution is used since authors believe it is sufficient to show the advantages of the proposed approach. For detailed validation of the same test case the reader is referred to Vukčević and Jasak 2015a. For the partitioned approach the solution generally converges with 8 or more PISO correctors. For most items, the monolithic approach exhibits convergence with smaller number of correctors, and significantly smaller deviations between the solutions using 2, 4 and 6 correctors. For most items the monolithic approach achieves solution that is closed to the converged value with only 2 correctors. Hence, the monolithic approach shows smaller sensitivity to the number of nonlinear correctors per time–step. The most important items from the practical point of view (C_{T0}, z_1 and ϕ_1) are virtually insensitive to the number of nonlinear correctors. Hence, savings in computational time can be achieved while retaining the same level of accuracy for this items by using fewer nonlinear correctors per time–step. The items that showed larger sensitivity to the number of nonlinear correctors are the mean of heave z_0, mean of pitch ϕ_0 and phase shift of pitch ϕ_1. The variation of mean of heave with the varying number of nonlinear correctors is similar for partitioned and monolithic approach. It is likely that the accuracy of fluid flow solution influences the result more than the accuracy of the pressure–rigid body motion coupling, which is indicated in Fig. 4. Mean of pitch, ϕ_0, has a very small absolute value, hence the absolute differences between the partitioned and monolithic approach are not large. Again, Fig. 7 shows that it takes more computational time

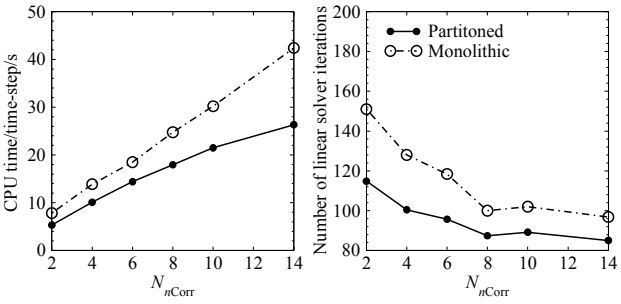

Fig. 7 Comparison of required computational time per time–step and the average number of pressure equation iterations with respect to the number of nonlinear correctors per time–step $N_{n\mathrm{Corr}}$

per time–step and more iterations of the pressure equation linear solver for the monolithic approach comparing to the partitioned approach.

Despite the fact that the monolithic approach requires more computational time per nonlinear corrector, significant savings can be achieved by using two instead of eight nonlinear correctors per time–step. According to Fig. 7, a reduction in overall computational time by a factor of 2.4 can be achieved in this manner.

5 Conclusions

Monolithic coupling of pressure equation and rigid body motion equations is shown in this paper for application in the field of computational marine hydrodynamics. The novel approach is first validated, and compared against the traditional partitioned approach in order to establish the validity and benefits of the method.

The validation is performed on a 2D heave decay simulation of a barge. The monolithic coupling approach is compared against the partitioned approach, showing very good agreement.

The performance of the two coupling methods is tested on a seakeeping case in regular head waves, where sensitivity to the number of pressure correctors per nonlinear corrector, as well as the number of nonlinear correctors per time step is investigated. Accuracy and computational time is compared for the two methods: monolithic coupling showed smaller sensitivity to the number of nonlinear correctors per time step, and it is shown that accurate results can be obtained with only two nonlinear correctors per time step. It is observed that the monolithic approach is computationally more expensive then the partitioned approach per nonlinear corrector, however it enables fewer nonlinear correctors to be used per time–step, offering a significant speed–up (by a factor of 2.4 for the given test case).

The developed monolithic coupling of pressure equation and rigid body motion is insensitive to the number of nonlinear correctors per time–step due to the better resolved coupling between the pressure equation and rigid body motion equations. The method offers significant savings in

computational time and is applicable in a wide range of problems in the field of marine hydrodynamics.

Acknowledgements

This research was sponsored by Bureau Veritas under the administration of Dr. Šime Malenica.

References

Bna S, Manservisi S, Aulisa E, 2013. A multilevel domain decomposition solver for monolithic fluid-structure interaction problems. *11th International Conference of Numerical Analysis and Applied Mathematics 2013*, Pts 1 and 2, Vol. 1558. Rhodes, 871-874.
DOI: 10.1063/1.4825635

Castiglione T, Stern F, Bova S, Kandasamy M, 2011. Numerical investigation of the seakeeping behavior of a catamaran advancing in regular head waves. *Ocean Engineering*, **38**, 1806-1822.
DOI: 10.1016/j.oceaneng.2011.09.003

Demirdžić I, Perić M, 1988. Space conservation law in finite volume calculations of fluid flow. *International Journal for Numerical Methods in Fluids*, **8**(9), 1037-1050.

Eken A, Sahin M, 2016. A parallel monolithic algorithm for the numerical simulation of large-scale fluid structure interaction problems. *International Journal for Numerical Methods in Fluids*, **80**(12), 687-714.
DOI: 10.1002/fld.4169

Farah P, Vuong AT, Wall WA, Popp A, 2016. Volumetric coupling approaches for multiphysics simulations on non-matching meshes. *International Journal for Numerical Methods in Engineering*, **108**(12), 1550-1576.
DOI: 10.1002/nme.5285

Hachem E, Feghali S, Codina R, Coupez T, 2013. Immersed stress method for fluidstructure interaction using anisotropic mesh adaptation. *International Journal for Numerical Methods in Engineering*, **94**(9), 805-825.
DOI: 10.1002/nme.4481

Heil M, Hazel AL, Boyle J, 2008. Solvers for large-displacement fluid-structure interaction problems: segregated versus monolithic approaches. *Computational Mechanics*, **43**(1), 91-101.
DOI: 10.1007/s00466-008-0270-6

Hu Z, Tang WY, Xue HX, Zhang XY, 2016. A simple-based monolithic implicit method for strong-coupled fluid-structure interaction problems with free surfaces. *Computer Methods in Applied Mechanics and Engineering*, **299**, 90-115.
DOI: 10.1016/j.cma.2015.09.011

Irons BM, Tuck RC, 1969. A version of the Aitken accelerator for computer iteration. *International Journal for Numerical Methods in Engineering*, **1**, 275-277.
DOI: 10.1002/nme.1620010306

Jasak H, 1996. *Error analysis and estimation for the finite volume method with applications to fluid flows*. PhD thesis, Imperial College of Science, Technology & Medicine, London.

Jasak H, Vukčević V, Gatin I, 2015. Numerical simulation of wave loads on static offshore structures. *CFD for Wind and Tidal Offshore Turbines*, 95-105.

Jog CS, Pal RK, 2011. A monolithic strategy for fluid-structure interaction problems. *International Journal for Numerical Methods in Engineering*, **85**(4), 429-460.
DOI: 10.1002/nme.2976

Langer U, Yang HD, 2016. Robust and efficient monolithic fluid-structure-interaction solvers. *International Journal for Numerical Methods in Engineering*, **108**(4), 303-325.
DOI: 10.1002/nme.5214

Larsson L, Stern F, Visonneau M, Hirata N, Hino T, Kim J, 2015. *Tokyo 2015: A Workshop on CFD in Ship Hydrodynamics*. Vol. 3, NMRI (National Maritime Research Institute), Tokyo, Japan.

Legay A, Zilian A, Janssen C, 2011. A rheological interface model and its space-time finite element formulation for fluid-structure interaction. *International Journal for Numerical Methods in Engineering*, **86**(6), 667-687.
DOI: 10.1002/nme.3060

Miyata H, Orihara H, Sato Y, 2014. Nonlinear ship waves and computational fluid dynamics. *Proceedings of the Japan Academy Series B—Physical and Biological Sciences*, **90**, 278-300.
DOI: 10.2183/pjab.90.278

Orihara H, Miyata H, 2003. Evaluation of added resistance in regular incident waves by computational fluid dynamics motion simulation using an overlapping grid system. *Journal of Marine Science and Technology*, **8**, 47-60.
DOI: 10.1007/s00773-003-0163-5

Press WH, Teukolsky SA, Vetterling WT, Flannery BP, 2002. *Numerical Recipes in C++: The Art of Scientific Computing*. Cambridge University Press, Cambridge.

Robinson-Mosher A, Schroeder C, Fedkiw R, 2011. A symmetric positive definite formulation for monolithic fluid structure interaction. *Journal of Computational Physics*, **230**(4), 1547-1566.
DOI: 10.1016/j.jcp.2010.11.021

Saad Y, 2003. *Iterative methods for sparse linear systems*. 2nd edition, Society for Industrial and Applied Mathematics Philadelphia.

Simonsen CD, Otzen JF, Joncquez S, Stern F, 2013. EFD and CFD for KCS heaving and pitching in regular head waves. *Journal of Marine Science and Technology*, **18**, 435-459.
DOI: 10.1007/s00773-013-0219-0

Tezdogan T, Demirel YK, Kellett P, Khorasanchi M, Incecik A, Turan O, 2015. Full-scale unsteady RANS CFD simulations of ship behaviour and performance in head seas due to slow steaming. *Ocean Engineering*, **97**, 186-206.
DOI: 10.1016/j.oceaneng.2015.01.011

Vukčević V, 2016. *Numerical modelling of coupled potential and viscous flow for marine applications*. PhD thesis, Faculty of Mechanical Engineering and Naval Architecture, University of Zagreb.

Vukčević V, Jasak H, 2015a. Seakeeping validation and verification using decomposition model based on embedded free surface method. *Tokyo 2015: A Workshop on CFD in Ship Hydrodynamics*.

Vukčević V, Jasak H, 2015b. Validation and verification of decomposition model based on embedded free surface method for oblique wave seakeeping simulations. *Tokyo 2015: A Workshop on CFD in Ship Hydrodynamics*.

Vukčević V, Jasak H, Gatin I, Malenica S, 2016. Seakeeping sensitivity studies using the decomposition CFD model based on the ghost fluid method. *Proceedings of the 31st Symposium on Naval Hydrodynamics*, Monterey.

Vukčević V, Jasak H, Malenica S, 2016a. Decomposition model for naval hydrodynamic applications, Part I: Computational method. *Ocean Eng.*, **121**, 37-46.
DOI: 10.1016/j.oceaneng.2016.05.022

Vukčević V, Jasak H, Malenica S, 2016b. Decomposition model for naval hydrodynamic applications, Part II: Verification and validation. *Ocean Eng.*, **121**, 76-88.
DOI: 10.1016/j.oceaneng.2016.05.021

Wu CS, Zhou DC, Gao L, Miao QM, 2011. CFD computation of ship motions and added resistance for a high speed trimaran in regular head waves. *International Journal of Naval Architecture and Ocean Engineering*, **3**, 105-110.
DOI: 10.3744/jnaoe.2011.3.1.105

Yang P, Xiang J, Fang F, Pavlidis D, Latham JP, Pain CC, 2016. Modelling of fluid-structure interaction with multiphase viscous flows using an immersed-body method. *Journal of Computational Physics*, **321**, 571-592.
DOI: 10.1016/j.jcp.2016.05.035